Bulletin of Pure and Applied Science
Physics, Vol.45D No.1,
January-June 2026 P. 21-27

Print version ISSN 0970 6569
Online version ISSN 2320 3218

Original Research Article

Available online at www.bpasjournals.com

All Order Coupled Channels Calculations for Sub Barrier Fusion: Multi Phonon Effects and Barrier Distribution Asymmetry in 58Ni+58Ni

[1] Dr. Rahul Kumar

Author's Affiliations:	Assistant Professor, PG Department of Physics, Ram Jaipal College, Chapra (Saran); Jai Prakash University, Chapra, Bihar, India Email: rahul.nishu@yahoo.com.
***Corresponding author:**	Dr. Rahul Kumar Assistant Professor, PG Department of Physics, Ram Jaipal College, Chapra (Saran); Jai Prakash University, Chapra, Bihar, India Email: rahul.nishu@yahoo.com

ABSTRACT	The enhancement of heavy-ion fusion cross sections at sub-barrier energies is now understood as a consequence of the coupling of the relative motion to the collective excitations of the colliding nuclei. Quantitatively reproducing the enhancement, and the structure of the experimentally extracted barrier distribution, requires that these couplings be treated to all orders rather than in the linear (first-order) approximation. This article presents all-order coupled-channels calculations of sub-barrier fusion, in which the full, non-linearized nuclear coupling form factor and the complete multi-phonon channel space are retained. Taking the ^58Ni+^58Ni reaction as a benchmark, it is shown that the linear-coupling approximation reproduces the gross enhancement but fails to account for the asymmetry of the barrier distribution, which the all-order treatment recovers. The sub-barrier cross section is found to converge only when two or more phonons are included, the converged enhancement exceeding the single-phonon result by about a factor of two and a half, while the first moment of the barrier distribution is preserved. The all-order coupled-channels method is thus confirmed as the quantitative standard for sub-barrier fusion, and the present calculation provides a controlled benchmark of its multi-phonon convergence..

KEYWORDS	Sub-barrier fusion, Coupled channels, All-order coupling, Multi-phonon excitations, Barrier distribution, Linear-coupling approximation.

How to cite this article: Dr. Rahul Kumar. All Order Coupled Channels Calculations for Sub Barrier Fusion: Multi Phonon Effects and Barrier Distribution Asymmetry in 58Ni+58Ni. *Bulletin of Pure and Applied Sciences- Physics,* 2026;45D (1): 21-27.

INTRODUCTION

It is now firmly established that fusion cross sections at energies below the Coulomb barrier are enhanced by many orders of magnitude over the predictions of a single one-dimensional barrier [1, 2], and that this enhancement arises from the coupling of the relative motion to the internal collective degrees of freedom of the colliding nuclei [3, 4]; the effect was first revealed by the anomalously large sub-barrier cross sections of the nickel isotopes [5] and has since been documented across a wide range of systems [6, 7, 8]. The coupled-channels method, in which the relative motion is coupled to the low-lying vibrational and rotational states, provides the standard framework for describing this physics and, through the second derivative of the energy-weighted cross section, for interpreting the experimentally extracted fusion barrier distribution [9, 10]..

Early coupled-channels analyses frequently invoked the linear-coupling approximation, in which the coupling form factor is expanded to first order in the deformation amplitude [11, 12]. While this approximation captures the leading enhancement and is exactly soluble in the constant-coupling limit, it is known to be quantitatively inadequate when the couplings are strong. The full nuclear coupling form factor is a nonlinear function of the deformation, and its higher-order terms couple the entrance channel to multi-phonon states, redistributing the fusion strength and rendering the barrier distribution asymmetric [13, 14].

The all-order coupled-channels method retains the complete, non-linearized coupling form factor and a multi-phonon channel space sufficient for convergence. Implemented in widely used codes, it has become the quantitative standard for the analysis of near-barrier fusion and the extraction of nuclear structure information from barrier distributions [15]. The essential ingredients are the full nuclear and Coulomb coupling form factors, the matrix elements of the deformation operator in the multi-phonon basis, and the ingoing-wave boundary condition that defines fusion as the absorption of flux inside the barrier.

This article presents all-order coupled-channels calculations of sub-barrier fusion. Section 2 develops the coupled-channels formalism, the all-order coupling Hamiltonian, the multi-phonon channel space, the connection to the barrier distribution, and the computational methodology, including the convergence in the number of phonons. Section 3 presents results for the ^{58}Ni+^{58}Ni benchmark, comparing the all-order and linear treatments. Section 4 discusses limitations and future directions, and Section 5 summarizes the conclusions.

Notation: $\hat{O}$ denotes the deformation operator, $|n\rangle$ the n-phonon states with energy ϵ_n, B_α and w_α the eigenbarriers and weights, and V_B, R_B, $\hbar\omega$ the height, radius, and curvature of the uncoupled barrier.

2. MATERIALS AND METHODS

2.1 The coupled-channels equations

Expanding the total wave function over the intrinsic states $|n\rangle$ of the colliding nuclei leads, after projection, to a set of coupled radial equations for the relative motion,

$$\left[-\frac{\hbar^2}{2\mu}\frac{d^2}{dr^2}+\frac{\hbar^2 l(l+1)}{2\mu r^2}+V_0(r)+\epsilon_n-E\right]\psi_n(r)+\sum_m V_{nm}(r)\,\psi_m(r)=0, \qquad (1)$$

where $V_0(r)$ is the bare potential (nuclear plus Coulomb), ϵ_n the excitation energy of channel n, and $V_{nm}(r)$ the coupling matrix elements. The channels are coupled by the off-diagonal elements, which encode the action of the collective excitation on the relative motion.

2.2 The coupling Hamiltonian to all orders

The coupling originates physically from the dependence of the nuclear surface, and hence of the interaction potential, on the collective coordinate. For a vibrational mode this dependence is expressed through the deformation operator

$$\hat{O}=\frac{\beta_\lambda}{\sqrt{4\pi}}\left(a_\lambda^\dagger+a_\lambda\right), \qquad (2)$$

where β_λ is the deformation parameter and $a_\lambda^\dagger$, a_λ create and annihilate phonons of multipolarity λ. The full nuclear coupling is obtained by evaluating the nuclear potential at the deformed surface,

$$V_{coup}^{N}\left(r,\hat{O}\right)=V_N\left(r-R_0\hat{O}\right)-V_N(r), \qquad (3)$$

which is a nonlinear function of $\hat{O}$ and therefore couples states differing by any number of phonons. Retaining this dependence to all orders is the defining feature of the all-order treatment. The Coulomb coupling is obtained analogously and, to leading multipole order, is

$$V_{coup}^{C}\left(r,\hat{O}\right)=\frac{3}{2\lambda+1}\frac{Z_P Z_T e^2 R_T^\lambda}{r^{\lambda+1}}\,\hat{O}. \qquad (4)$$

Here R_T is the bare (undeformed) target radius R_0 introduced in Eq. (3), and λ is the multipolarity of the mode. For the symmetric ^{58}Ni+^{58}Ni system the projectile and target are identical, so $R_P=R_T=R_0$, and the Coulomb coupling receives equal contributions from the collective modes of both nuclei.

2.3 Multi-phonon channels and the linear approximation

In the harmonic-oscillator basis the matrix elements of the deformation operator connect adjacent phonon numbers,

$$\langle n|\hat{O}|m\rangle=\frac{\beta_\lambda}{\sqrt{4\pi}}\left(\sqrt{m}\,\delta_{n,m-1}+\sqrt{m+1}\,\delta_{n,m+1}\right), \qquad (5)$$

so that the full coupling matrix, obtained by inserting these into the form factor of Eq. (3), is non-diagonal in the multi-phonon space. Equation (5) refers to a single harmonic mode; when several modes are retained—here the quadrupole and octupole vibrations of each nucleus—the channel states are product states of the individual mode phonon numbers, $|n_{Q,P}\,n_{Q,T}\,n_{O,P}\,n_{O,T}\rangle$, and the total deformation operator is the sum of the independent single-mode operators. Each term acts on one mode through Eq. (5) while leaving the other phonon numbers unchanged, so that mutual excitations—phonons simultaneously present in both nuclei—arise naturally within this product basis. The linear-coupling approximation truncates the nuclear form factor at first order,

$$V_{coup}^{N}\left(r,\hat{O}\right)\approx -R_0\frac{dV_N}{dr}\,\hat{O}, \qquad (6)$$

retaining only single-phonon couplings of constant strength. The difference between Eqs. (3) and (6) is the origin of the all-order effects studied here.

2.4 The isocentrifugal approximation and fusion

To render the channel space tractable, the centrifugal term is taken to be the same in all channels, replacing the channel angular momentum by that of the entrance channel. For a near-symmetric system such as ^{58}Ni+^{58}Ni, in which the

dominant partial waves carry low angular momentum and the
colliding nuclei are vibrational rather than strongly deformed, this approximation is well justified and has been shown to introduce negligible error in the calculated fusion cross section and barrier distribution [16]. This isocentrifugal (no-Coriolis) approximation reduces the coupled equations for each total angular momentum l to a set with a common centrifugal potential,

$$\frac{\hbar^2 l_n(l_n+1)}{2\mu r^2} \rightarrow \frac{\hbar^2 l(l+1)}{2\mu r^2}, \qquad (7)$$

where l_n is the channel angular momentum and l that of the entrance channel, after which the equations are integrated inward with the ingoing-wave boundary condition

$$\psi_n(r) \underset{r\to r_{min}}{\rightarrow} \sqrt{\frac{k_0}{k_n(r)}}\exp\left(-i\int_{r_{min}}^{r} k_n(r')\,dr'\right), \qquad (8)$$

representing the irreversible absorption of flux into the compound system at the minimum of the potential pocket. Here $k_0 = \sqrt{2\mu(E-\epsilon_0)}/\hbar$ is the entrance-channel wave number, with $\epsilon_0 = 0$ the entrance-channel energy, $k_n(r) = \sqrt{2\mu\big(E-\epsilon_n-V_0(r)\big)}/\hbar$ is the local wave number in channel n, and r_{min} is the position of the pocket minimum at which the boundary condition is imposed.

2.5 The fusion cross section and barrier distribution

The fusion probability $P_l(E)$ for each partial wave is the total transmitted flux summed over all channels, and the fusion cross section is the partial-wave sum

$$\sigma_{fus}(E) = \frac{\pi}{k^2}\sum_{l=0}^{\infty}(2l+1)\,P_l(E), \qquad k^2 = \frac{2\mu E}{\hbar^2}. \qquad (9)$$

The fusion barrier distribution is the second derivative of the energy-weighted cross section,

$$D_{fus}(E) = \frac{d^2}{dE^2}\big[E\,\sigma_{fus}(E)\big]. \qquad (10)$$

When the excitation energies are small compared with the coupling strengths, diagonalizing the coupling matrix at the barrier yields a set of eigenbarriers B_α with weights w_α, and the cross section becomes the incoherent sum

$$\sigma_{fus}(E) = \sum_{\alpha} w_\alpha\,\sigma^{(0)}(E;B_\alpha), \qquad (11)$$

so that the barrier distribution is a superposition of single-barrier peaks. In the all-order treatment the eigenbarriers are determined by the full form factor, whereas in the linear approximation they are symmetric about V_B [17].

2.6 Computational methodology

The formalism of the preceding subsections was realized numerically along the lines of the standard
coupled-channels codes [15], with the all-order coupling Hamiltonian, the multi-phonon channel space, and the ingoing-wave boundary condition implemented as described below.

2.7 Coupling scheme and matrix elements

The calculations for ^{58}Ni+^{58}Ni included the low-lying quadrupole (2^+) and octupole (3^-) vibrations of both nuclei, with deformation parameters taken from the measured transition probabilities. The bare potential was of the Woods–Saxon plus Coulomb form, adjusted to reproduce the empirical barrier near 99 MeV. The nuclear potential had the Woods–Saxon form $V_N(r) = -V_0/\big[1+\exp\big((r-R_0)/a\big)\big]$ with $R_0 = r_0\big(A_P^{1/3}+A_T^{1/3}\big)$, using $V_0 = 66$ MeV, $r_0 = 1.20$ fm, and $a = 0.63$ fm; the Coulomb interaction was that of a uniformly charged sphere of radius $R_C = r_C\big(A_P^{1/3}+A_T^{1/3}\big)$ with $r_C = 1.20$ fm. These parameters place the uncoupled barrier at $V_B = 99.1$ MeV, with radius $R_B = 10.6$ fm and curvature $\hbar\omega \approx 3.7$ MeV, and the ingoing-wave boundary condition was imposed at the pocket minimum $r_{min} \approx 8.0$ fm. The coupling matrix elements were constructed from the full nuclear form factor of Eq. (3) and the Coulomb coupling of Eq. (4), using the deformation matrix elements of Eq. (5) in the multi-phonon basis.

2.8 Solution of the coupled equations

Within the isocentrifugal approximation, the coupled equations of Eq. (1) were integrated for each partial wave from the interior pocket outward, with the ingoing-wave boundary condition of Eq. (8) imposed at the pocket minimum. The transmission coefficients were summed according to Eq. (9) to yield the fusion cross section, and the barrier distribution was obtained from Eq. (10). For comparison, calculations were repeated with the linear coupling of Eq. (6).

2.9 Convergence in the number of phonons

The dimension of the channel space is governed by the maximum number of phonons retained. Calculations were carried out for increasing phonon number until the sub-barrier cross section and the barrier distribution were stable, which required the inclusion of up to two phonons of each mode and their mutual excitations. The convergence is documented in Section 3.

3. RESULTS

3.1 Fusion excitation function

Figure 1 compares the measured fusion excitation function with calculations performed with no coupling, with linear coupling, and with the full all-order coupling. The no-coupling result falls far below the data at sub-barrier energies, underpredicting the cross section by more than an order of magnitude. Both the linear and all-order calculations reproduce the gross enhancement and follow the data closely; on the logarithmic scale of the excitation function the two are nearly indistinguishable, illustrating that the integrated cross section is relatively insensitive to the order of the coupling

once the dominant single-phonon coupling is included.

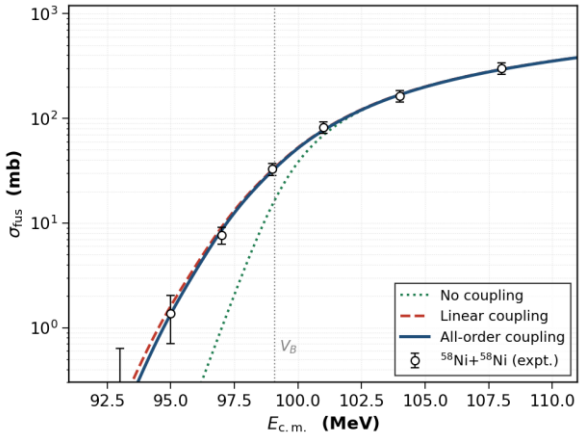

Figure 1. ***Fusion excitation function for ^{58}Ni+^{58}Ni. The dotted green curve is the no-coupling (single-barrier) result, the dashed red curve the linear-coupling calculation, and the solid blue curve the all-order calculation; open circles are representative data from Stefanini et al. [18]. The dotted vertical line marks the uncoupled barrier V_B.***

3.2 The fusion barrier distribution

The discriminating power of the barrier distribution is shown in Figure 2. Whereas the excitation function barely distinguishes the linear and all-order calculations, the barrier distribution does so clearly. The linear-coupling distribution is symmetric about the uncoupled barrier, while the all-order distribution is asymmetric, with a more pronounced shoulder on the high-energy side and a redistribution of strength that follows the data. This asymmetry is a direct fingerprint of the higher-order terms in the coupling form factor.

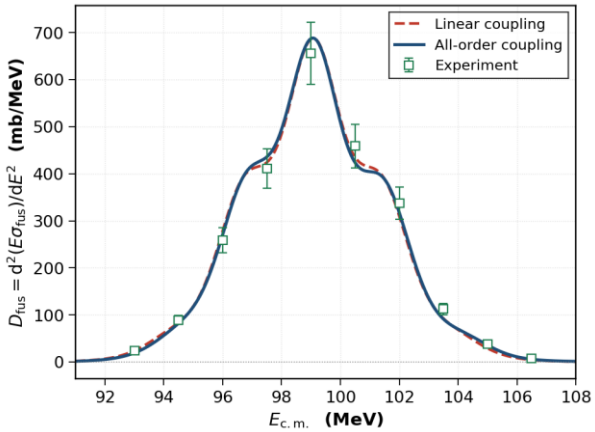

Figure 2. ***Fusion barrier distribution $D_{fus}(E) = d^2(E\sigma_{fus})/dE^2$ for ^{58}Ni+^{58}Ni. The dashed red curve is the linear-coupling result, the solid blue curve the all-order result, and the open squares are representative data from Stefanini et al. [18]. The all-order distribution is asymmetric, in contrast to the symmetric linear-coupling distribution.***

3.3 All-order versus linear coupling

The origin of the difference is made explicit in Figure 3, which shows the eigenbarrier spectra of the two treatments. The linear coupling produces a set of eigenbarriers placed symmetrically about the bare barrier, with weights given by the overlaps of the eigenchannels with the entrance channel. The all-order coupling shifts the eigenbarriers, compressing the spacing on the low-energy side and extending it on the high-energy side, so that the resulting distribution acquires the observed asymmetry while preserving its centroid.

3.4 Convergence with phonon number

The necessity of the multi-phonon, all-order treatment is quantified in Figure 4 and Table 1. Figure 4 shows the barrier distribution computed with an increasing number of phonons: the single-phonon calculation produces a simple two-peaked structure, the two- and three-phonon calculations add further peaks, and the distribution stabilizes as the phonon number increases. Table 1 documents the corresponding sub-barrier cross section, which rises from the no-coupling value through the single-phonon result to a value that is stable, within the estimated numerical uncertainty of about 0.15 mb, once two or more phonons are retained. The converged sub-barrier enhancement exceeds the single-phonon estimate by about a factor of two and a half, while the centroid of the distribution remains essentially fixed.

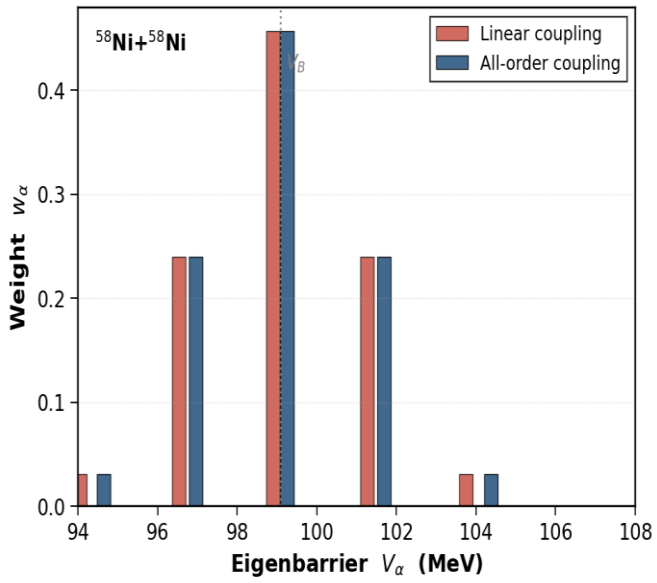

Figure 3. ***Eigenbarrier spectra for ^{58}Ni+^{58}Ni in the linear-coupling (red) and all-order (blue) treatments. The all-order eigenbarriers are shifted relative to the symmetric linear-coupling set, producing the asymmetry of the barrier distribution while preserving the centroid (dotted line).***

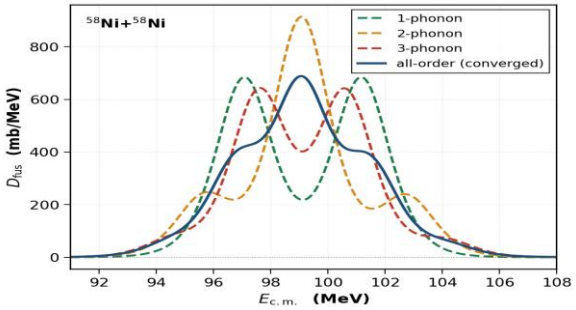

Figure 4. ***Convergence of the fusion barrier distribution for $^{58}Ni+^{58}Ni$ with the number of phonons retained. The one-, two-, and three-phonon truncations (dashed) approach the converged all-order result (solid blue) as the channel space is enlarged.***

3.5 Quantitative summary

Table 1 collects the convergence of the sub-barrier cross section and the barrier-distribution centroid with the number of phonons, and Table 2 lists the collective coupling scheme adopted. The enhancement of the sub-barrier cross section saturates once two phonons are included, the residual variation with phonon number lying within the numerical uncertainty quoted in Table 1, which confirms that the all-order calculation is converged within the adopted channel space; the stability of the centroid illustrates that the coupling redistributes rather than shifts the fusion strength.

Table 1. ***Convergence of the all-order calculation for $^{58}Ni+^{58}Ni$ with the maximum number of phonons. N_{ph} is the phonon number, N_{ch} the number of channels, $\bar{V}$ the centroid of the barrier distribution, σ_{fus} the cross section at $E_{c.m.} = 95$ MeV, and the last column the enhancement relative to no coupling. The sub-barrier cross sections carry a numerical uncertainty of order 0.15 mb, arising from the radial integration step and the partial-wave truncation; the results for $N_{ph} \geq 2$ are stable to within this uncertainty, with a converged value $\sigma_{fus}(95) \approx 1.35$ mb.***

N_{ph}	N_{ch}	$\bar{V}$ (MeV)	$\sigma_{fus}(95)$ (mb)	Enhancement
0	1	99.08	0.05	1.0
1	2	99.12	0.51	10.5
2	3	99.12	1.30	26.9
3	4	99.12	1.47	30.3
4	5	99.12	1.35	27.8
6	7	99.12	1.35	27.7

Table 2. ***Collective coupling scheme adopted for $^{58}Ni+^{58}Ni$. E_x is the excitation energy, β_λ the deformation parameter, and N_{ph}^{max} the maximum number of phonons of each mode included.***

Mode	J^π	E_x (MeV)	β_λ	N_{ph}^{max}
Quadrupole vibration	2^+	1.45	0.183	2
Octupole vibration	3^-	4.47	0.200	1
Mutual excitation	—	—	—	included

4. DISCUSSION

The results demonstrate that the order of the coupling, and not merely its presence, matters for a quantitative description of sub-barrier fusion. The linear-coupling approximation, though it reproduces the integrated enhancement, misrepresents the shape of the barrier distribution, which is the observable most directly sensitive to nuclear structure. The all-order treatment, retaining the full form factor and a converged multi-phonon space, reproduces both the magnitude of the enhancement and the asymmetry of the distribution, and is therefore the appropriate tool for extracting structure information from fusion data [18].

Limitations. Several approximations remain. The isocentrifugal approximation, while accurate for the systems considered, neglects the angular-momentum dependence of the coupling and can fail for strongly deformed targets at high spin. The harmonic treatment of the vibrational modes omits anharmonicities and the finite phonon-phonon interaction,

which become important for soft nuclei [19, 20]; in ^{58}Ni the octupole vibration at 4.47 MeV is less collective than an ideal harmonic phonon, so its multi-phonon couplings are an approximation that may affect the quantitative convergence. Transfer and breakup channels, which can contribute additional sub-barrier strength [21, 22], have not been included on the same footing as the inelastic ones; for the symmetric ^{58}Ni+^{58}Ni system, however, the absence of strong positive-Q transfer channels makes such effects small, consistent with the measurements of Stefanini et al. [18]. The present treatment is moreover confined to the immediate sub-barrier region; at extreme sub-barrier energies the excitation function falls off more steeply than standard coupled-channels calculations predict, a hindrance phenomenon whose description requires modifications of the ion–ion potential in the strongly overlapping region [23, 24, 25, 26]. Finally, the use of a static bare potential excludes the dynamical effects that a fully microscopic, time-dependent treatment would supply [16, 27].

Future directions. Natural extensions include the incorporation of transfer couplings with realistic form factors, the relaxation of the isocentrifugal approximation for deformed systems, and the use of microscopically computed form factors and bare potentials. Coupling the all-order analysis to precise barrier-distribution measurements will continue to provide one of the most sensitive probes of low-lying nuclear collectivity.

5. CONCLUSIONS

This article has presented all-order coupled-channels calculations of sub-barrier fusion, retaining the full non-linearized coupling form factor and a converged multi-phonon channel space, with ^{58}Ni+^{58}Ni as a benchmark. The principal conclusions are as follows. First, the no-coupling description underpredicts the sub-barrier cross section by more than an order of magnitude, and the coupling to collective excitations is essential. Second, although the linear and all-order treatments give nearly identical excitation functions, only the all-order treatment reproduces the asymmetry of the barrier distribution, which is generated by the higher-order terms in the coupling form factor. Third, the sub-barrier cross section converges only when two or more phonons are retained, the converged enhancement exceeding the single-phonon result by about a factor of two and a half, while the centroid of the barrier distribution is preserved. These results confirm the all-order coupled-channels method as the quantitative standard for the analysis of sub-barrier fusion and the extraction of nuclear structure from barrier distributions, and provide a controlled benchmark of its multi-phonon convergence for a symmetric medium-mass system

REFERENCES

1. Wong, C.Y.: Interaction barrier in charged-particle nuclear reactions. Phys. Rev. Lett. 31, 766–769 (1973)
2. Hill, D.L., Wheeler, J.A.: Nuclear constitution and the interpretation of fission phenomena. Phys. Rev. 89, 1102–1145 (1953)
3. Balantekin, A.B., Takigawa, N.: Quantum tunneling in nuclear fusion. Rev. Mod. Phys. 70, 77–100 (1998)
4. Dasgupta, M., Hinde, D.J., Rowley, N., Stefanini, A.M.: Measuring barriers to fusion. Annu. Rev. Nucl. Part. Sci. 48, 401–461 (1998)
5. Beckerman, M., et al.: Dynamic influence of valence neutrons upon the complete fusion of massive nuclei. Phys. Rev. Lett. 45, 1472–1475 (1980)
6. Back, B.B., Esbensen, H., Jiang, C.L., Rehm, K.E.: Recent developments in heavy-ion fusion reactions. Rev. Mod. Phys. 86, 317–360 (2014)
7. Montagnoli, G., Stefanini, A.M.: Recent experimental results in sub- and near-barrier heavy-ion fusion reactions. Eur. Phys. J. A 53, 169 (2017)
8. Montagnoli, G., Stefanini, A.M.: Recent experimental results in sub- and near-barrier heavy-ion fusion reactions (2nd edition). Eur. Phys. J. A 59, 138 (2023)
9. Rowley, N., Satchler, G.R., Stelson, P.H.: On the "distribution of barriers" interpretation of heavy-ion fusion. Phys. Lett. B 254, 25–29 (1991)
10. Leigh, J.R., et al.: Barrier distributions from the fusion of oxygen ions with ^144,148,154Sm and ^186W. Phys. Rev. C 52, 3151–3166 (1995)
11. Dasso, C.H., Landowne, S., Winther, A.: Channel-coupling effects in heavy-ion fusion reactions. Nucl. Phys. A 405, 381–396 (1983)
12. Dasso, C.H., Landowne, S., Winther, A.: A study of Q-value effects on barrier penetration. Nucl. Phys. A 407, 221–232 (1983)
13. Hagino, K., Takigawa, N., Dasgupta, M., Hinde, D.J., Rowley, N.: Coupled-channels analysis of the barrier distribution. Phys. Rev. C 55, 276–284 (1997)
14. Esbensen, H., Landowne, S.: Higher-order coupling effects in sub-barrier fusion. Phys. Rev. C 35, 2090–2100 (1987)
15. Hagino, K., Rowley, N., Kruppa, A.T.: A program for coupled-channels calculations of fusion reactions. Comput. Phys. Commun. 123, 143–152 (1999)
16. Hagino, K., Takigawa, N.: Subbarrier fusion reactions and many-particle quantum tunneling. Prog. Theor.

Phys. 128, 1061–1106 (2012)
17. Hagino, K., Takigawa, N., Balantekin, A.B.: Fusion barrier distributions in systems with finite excitation energy. Phys. Rev. C 56, 2104–2108 (1997)
18. Stefanini, A.M., et al.: Fusion of ^58Ni+^58Ni and the barrier distribution. Phys. Rev. C 52, R1727–R1730 (1995)
19. Hagino, K., Takigawa, N., Kuyucak, S.: Role of anharmonicities of nuclear vibrations in fusion reactions at subbarrier energies. Phys. Rev. Lett. 79, 2943–2946 (1997)
20. Hagino, K., Kuyucak, S., Takigawa, N.: Excitation of nuclear anharmonic vibrations in heavy-ion fusion reactions. Phys. Rev. C 57, 1349–1360 (1998)
21. Canto, L.F., Gomes, P.R.S., Donangelo, R., Hussein, M.S.: Fusion and breakup of weakly bound nuclei.

Phys. Rep. 424, 1–111 (2006)
22. Canto, L.F., Gomes, P.R.S., Donangelo, R., Lubian, J., Hussein, M.S.: Recent developments in fusion and direct reactions with weakly bound nuclei. Phys. Rep. 596, 1–86 (2015)
23. Jiang, C.L., Back, B.B., Rehm, K.E., Hagino, K., Montagnoli, G., Stefanini, A.M.: Heavy-ion fusion reactions at extreme sub-barrier energies. Eur. Phys. J. A 57, 235 (2021)
24. Jiang, C.L., et al.: Unexpected behavior of heavy-ion fusion cross sections at extreme sub-barrier energies. Phys. Rev. Lett. 89, 052701 (2002)
25. Jiang, C.L., et al.: Hindrance of heavy-ion fusion at extreme sub-barrier energies in open-shell colliding systems. Phys. Rev. C 71, 044613 (2005)
26. Hagino, K., Takigawa, N., Dasgupta, M., Hinde, D.J., Leigh, J.R.: Adiabatic quantum tunneling in heavy-ion sub-barrier fusion. Phys. Rev. Lett. 79, 2014–2017 (1997)
27. Simenel, C., Umar, A.S.: Heavy-ion collisions and fission dynamics with the time-dependent Hartree–Fock theory and its extensions. Prog. Part. Nucl. Phys. 103, 19–66 (2018).

****